CORA Cork Open Research Archive
Cartlann Taighde Oscailte Chorcaí

Title	Fabrication of arrays of lead zirconate titanate (PZT) nanodots via block copolymer self-assembly
Authors	Varghese, Justin M.;Ghoshal, Tandra;Deepak, Nitin;O'Regan, Colm;Whatmore, Roger W.;Morris, Michael A.;Holmes, Justin D.
Publication date	2013-02-18
Original Citation	VARGHESE, J., GHOSHAL, T., DEEPAK, N., O'REGAN, C., WHATMORE, R. W., MORRIS, M. A. & HOLMES, J. D. 2013. Fabrication of Arrays of Lead Zirconate Titanate (PZT) Nanodots via Block Copolymer Self-Assembly. Chemistry of Materials, 25, 1458-1463. http://dx.doi.org/10.1021/cm303759r
Type of publication	Article (peer-reviewed)
Link to publisher's version	http://pubs.acs.org/doi/pdf/10.1021/cm303759r - 10.1021/cm303759r
Rights	© 2013 American Chemical Society. This document is the Accepted Manuscript version of a Published Work that appeared in final form in Chemistry of Materials, copyright © American Chemical Society after peer review and technical editing by the publisher. To access the final edited and published work see http://pubs.acs.org/doi/pdf/10.1021/cm303759r
Download date	2026-10-28 14:08:44
Item downloaded from	https://hdl.handle.net/10468/2272

UCC
University College Cork, Ireland
Coláiste na hOllscoile Corcaigh

Fabrication of Arrays of PZT Nanodots via Block Copolymer Self-Assembly

Justin Varghese, [§, †, ǁ] Tandra Ghoshal, [§, †, ǁ] Nitin Deepak, [†] Colm O'Regan, [§, †, ǁ] Roger W. Whatmore, [†] Michael A. Morris[§, †, ǁ] and Justin D. Holmes *, [§, †, ǁ]

[§]Materials Chemistry and Analysis Group, Department of Chemistry, University College Cork, Cork, Ireland.

[†]Tyndall National Institute, University College Cork, Lee Maltings, Dyke Parade, Cork, Ireland.

[ǁ]Centre for Research on Adaptive Nanostructures and Nanodevices (CRANN), Trinity College Dublin, Dublin 2, Ireland.

KEYWORDS : PZT, Block copolymer, PFM, nanodot, piezoelectric

ABSTRACT: This article presents a simple methodology for the fabrication of two dimensional arrays of lead zirconate titanate (PZT) nanodots on n-doped Si substrates via the directed self-assembly of PS-*b*-PEO block copolymer templates. The approach produces highly ordered PZT nanodot patterns, with lateral widths and heights as small as 20 and 10 nm respectively, and a coverage density as high as ~ 68 × 10^9 nanodots cm^{-2}. The existence of a pervoskite phase in the nanodots was confirmed by X-ray diffraction and X-ray photoelectron spectroscopy. The piezo-amplitude and ferroelectric domain response obtained from the nanodots, through piezoresponse force microscopy, confirmed the presence of ferroelectricity in the PZT arrays. Notably, PZT nanodots with a thickness ~ 10 nm, which is close to the critical size limit of PZT, showed ferroelectric behavior. The presence of a multi-a/c domain structure in the nanodots was attributed to their polycrystalline nature.

INTRODUCTION

The continuing miniaturization of ferroelectric-based memories requires the creation of isolated nanosized ferroelectric domains (< 100 nm) to achieve ultra-high density ferroelectric memory units.[1-7] Efforts have been made by a number of research groups to realize this goal by nanoscaling ferroelectric materials using different 'top-down' and 'bottom-up' approaches.[3,8-10] Fabrication of two dimensional (2D) arrays of ferroelectric nanoislands or nanodots is an ideal approach for forming isolated nanodomains, where the individual units can store physically separate bits of data.[3,5,6,8,11] Isolated single-crystalline ferroelectric nanostructures have shown improved memory characteristics such as high polarization retention compared to their thin film counterparts, due to the presence of single ferroelectric domains,[11] and increased electromechanical displacement due the reduction of clamping effects on 90 degree domain reorientation.[12] Techniques such as electron beam lithography,[5,6] focused ion beam milling,[12] nanoimprint lithography,[13,14] dip-pen lithography,[15] sol-gel self-assembly[16-18] and templating[7,11,19-21] have been used successfully to fabricate arrays of discrete nanoislands or dots. Although 'top-down' lithography-based techniques have been successful in making precisely positioned ferroelectric nanodots, their inherent feature-size limitations, low throughput and high processing cost makes these techniques less prevalent.[22] While self-assembly-based 'bottom-up' methods offer facile high-throughput synthesis of ferroelectric nanoislands, they suffer from poor ordering and limited control over feature size, which limits their practical application.[16-18,22] Template-assisted synthesis is a simplistic low-cost route for fabricating ferroelectric nanodots, due to the number of deposition methods that can be utilized and good control over the dimensions of the nanostructures formed.[7,11,19-21] For example, Lee et al.[3] fabricated individually addressable epitaxial arrays of PZT nanodot capacitors (~ 60 nm in diameter and ~ 20 to 40 nm in height) with a density of 32 Gb cm^{-2} using anodic aluminium oxide (AAO) templates. However, the use of AAO as a template is limited, due to the difficulty in forming membranes on desired substrates and typically poor ordering at low dimensions (< 50 nm). Nanosphere lithography (NSL) has also been used to obtain 2D ferroelectric nanostructures, but the minimum feature size that could be achieved by this method was limited to ~ 50 nm.[15-17]

Block copolymer (BCP) based self-assembly has emerged as a viable 'bottom-up' patterning technique for nanostructures, due to the ability to form different types of 2D and 3D nanoscale patterns on various substrates.[23,24] These self-assembled patterns have been used as nanolithographic masks, as well as templates for the fabrication of arrays of dots and wires of inorganic organic nanostructures.[23,24] The capabilities of BCP patterning techniques therefore have the potential to generate ordered arrays of ferroelectric nanodots and nanowires. The use of self-assembled BCPs to produce ferroelectric nanostructures is still in its infancy and has not yet been fully explored. Diblock copolymers have been the most widely used for creating self-assembled patterns of nanostructures.[23,24] Kang et al.[8] used polystyrene-block-poly(ethyleneoxide) (PS-*b*-PEO) diblock polymer templates for the confined crystallization of the ferroelectric polymer PVDF-TrFE into periodically aligned nanowire patterns trenches, 30 nm in width and 50 nm in periodicity. Zoelen et

al.[25] used polystyrene-block-poly(4-vinyl pyridine) [PS-*b*-P4VP] for the fabrication of line patterns of $PbTiO_3$ nanoparticles, with a mean height ~ 25 nm and periodicity ~ 65 nm. Kim et al.[26] prepared high-density arrays of $PbTiO_3$ nanodots, with mean heights of 7 nm and diameters of 22 nm, using the self-assembled BCP PS-*b*-P4VP. To form $PbTiO_3$ nanodot patterns, the former group employed pulsed laser deposition on PS-*b*-P4VP lamellae, whilst the latter group utilized micelle-based incorporation of a $PbTiO_3$ precursor into the PS-*b*-P4VP thin film, due to the favorable interaction of the precursor with the polar P4VP polymer block. The interaction of metallic precursors towards the P4VP polar block in PS-*b*-P4VP occurred due to the selective co-ordination of the metal ions (Pb^{2+} and Ti^{4+}) with the polar functional moiety (pyridine) present in the block. Similar interactions have been reported in the fabrication of arrays of iron oxide nanoparticles using polystyrene-block-polyethylene oxide (PS-*b*-PEO) thin films.[27] This metal ion impregnation method has great potential for generating ferroelectric nanostructures in a single step, without the requirement for polymer etching, as the annealing process not only crystallizes the nanostructures but also removes the polymer.

This article reports the synthesis of highly ordered 2D arrays of PZT ($PbZr_{0.3}Ti_{0.7}O_3$) [PZT 30/70] nanodots using self-assembled PS-*b*-PEO thin films. PZT 30/70 composition was studied due to its commercial importance and its excellent piezoelectric and ferroelectric characteristics,[28] especially in thin film form.[29,30] Piezoresponse force microscopy (PFM) provided an ideal technique for probing the nanoscale ferroelectric and piezoelectric properties of arrays of PZT nanodots[12] produced.

EXPERIMENTAL

Polystyrene-block-polyethylene oxide (PS-*b*-PEO) was purchased from Polymer Sources, Canada and used without further purification. Nanodot templates, of various diameters and spacing, were obtained using two different number average molecular weights (Mn) of PS-*b*-PEO; 42-11.5 (Mn, PS = 42 kg mol^{-1}; Mn, PEO = 11.5 kg mol^{-1}; Mw/Mn = 1.07 (Mw: weight-average molecular weight) and 32-11 (Mn, PS = 32 kg mol^{-1}; Mn, PEO = 11 kg mol^{-1}; Mw/Mn = 1.06). N-doped silicon substrates were used for the deposition of PZT. Substrates were cleaned by ultrasonication in acetone and toluene, for 30 min in each solvent, and dried under N_2. The process of making PS-*b*-PEO templates was adopted from the previous work reported by Ghoshal et al.[27]

PZT precursor solutions was formulated using lead (II) acetate ($Pb(CH_3COO)_2{\cdot}3H_2O$), zirconium (IV) acetylacetonate or Zr(acac) and titanium (IV) isopropoxide as starting materials. The transferring, weighing and mixing of the chemicals was done inside an inert atmosphere glove-box to avoid hydrolysis. Lead acetate (0.158 mmol; an excess of 10 % lead acetate was used in order to compensate for the loss of Pb during annealing) was dissolved in 2 ml of glacial acetic acid. Zr(acac) (0.042 mmol) and titanium isopropoxide (0.099 mmol) were dissolved in 8 ml of anhydrous ethanol. This solution was mixed with the acidified lead acetate solution to obtain a PZT precursor solution with a Zr/Ti ratio of 30/70. Dilute solutions of titanium isopropoxide (0.015 mmol) in anhydrous ethanol were then spin coated (6000 rpm for 10 s) onto the PS-*b*-PEO template and left at room temperature overnight to obtain a thin amorphous layer of TiO_2; which helped to prevent the diffusion of Pb into the Si substrate and also enhanced the formation of pervoskite PZT.[31] The PZT precursor solution was then spin coated onto this PS-*b*-PEO film at 3000 rpm for 30 s. In order to oxidize the precursor and to remove the polymer, UV/Ozone treatment (PSD Pro Series Digital UV Ozone System; Novascan Technologies, Inc., USA) was carried out on precursor-loaded templates for 2 h. Further crystallization of the PZT nanodots was achieved by annealing the pre-oxidized samples at 600 °C for 1 h.

The morphological characterization of PZT nanodot samples was performed using a FEI Quanta 650 FEG-SEM and on a JEOL-JEM 2100 TEM operated at 200 kV. X-ray diffraction (XRD) patterns of PZT nanodots was collected on a Philips X'Pert diffractometer using Cu Kα1 radiation with an anode current of 35 mA and an accelerating voltage of 40 kV over the angle range $2\theta = 20$ to 40°, using a step size of 0.01 and a scan rate 0.05. X-ray photoelectron spectroscopy (XPS) analysis of the samples was performed on a VSW Atomtech system with twin anode (Al/Mg) X-ray source. Survey spectra were collected at a pass-energy of 100 eV, a step size of 0.7 eV and a dwell time of 100 µs. Core-level spectra were acquired as an average of 15 scans at a pass-energy of 50 eV, a step size of 0.2 eV and a dwell time of 100 µs. The core-level spectra of each element were deconvoluted and fitted using VSW spectra presenter software (version 8.0-B-2). The ferroelectric and piezoelectric properties of arrays of PZT nanodots were analyzed by SS-PFM (MFP-3D™ software, Asylum Research, Santa Barbara, CA) using a conductive cantilever (AC240TM Pt coated silicon probe, Olympus).

RESULTS AND DISCUSSION

Self-assembled thin films of PS-*b*-PEO (42-11.5) were fabricated on n-doped Si substrates by spin coating the polymer solution onto the substrate followed by solvent annealing and ethanol treatment[27]; (42-11.5) stands for the number average molecular weight in kg $mol^{-1}$of PS and PEO block respectively. Figures 1(a) and (b) shows scanning electron microscopy (SEM) images of self-assembled PS-*b*-PEO (42-11.5) thin films formed on Si substrates; the bright contrast represents the PS block and the dark contrast represents the PEO block. The hydrophilic PEO block phase separates from the hydrophobic PS block in the form of cylindrical domains. The center-to-center cylinder spacing in the phase separated polymer was ~ 42 nm, with a mean PEO cylindrical diameter ~ 19.3 nm and film thickness of ~ 40 nm. Arrays of PZT nanodots were formed by the simple inclusion of the PZT precursor solution into the PEO component of the thin film via spin coating, followed by UV/ozone treatment to completely remove the polymers. As shown in Figures 1(c) and (d), well-ordered arrays of isolated PZT nanodots with diameter around 30 ± 5 nm were fabricated on an n-doped Si substrate. Close examination of the SEM images revealed that isolated nanodots formed, with only few dots being interconnected. The placement of the nanodots mimicked the original self-assembled block copolymer pattern. The cross-sectional transmission electron microscopy (TEM) image, Figure 1(d) inset, of the PZT nanodots formed further confirmed that the nanodots were isolated and had an average height of ~15 nm. The mean thickness and diameter of the PZT nanodots fabricated using the PS-*b*-PEO (42-11.5) BCP were less than half the dimensions previously reported by Lee *et al.*[3] Isolated arrays of PZT nanodots are ideal for the formation of individ-

ual ferroelectric domains to achieve high storage density in memory applications.[3,5,6,11] The PZT nanodots fabricated using PS-*b*-PEO (42-11.5) had a coverage density 42 × 10^9 nanodots cm^{-2} which in turn gives a memory density of 42 Gb cm^{-2}, which is greater than that previously reported.[3]

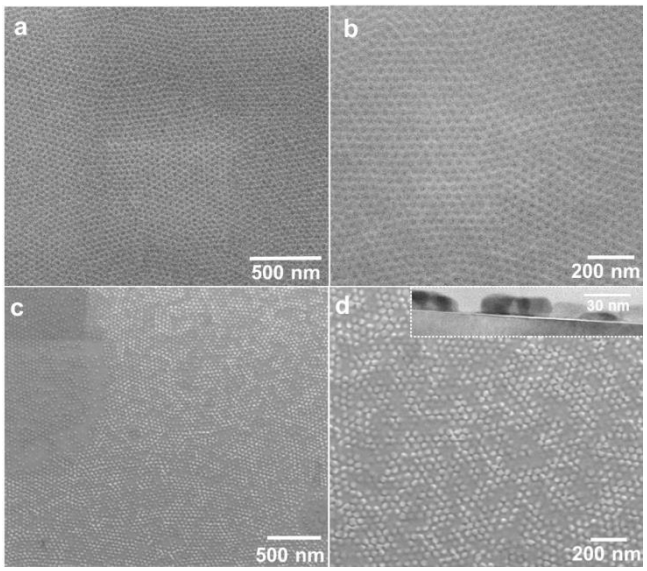

Figure 1. Plan-view SEM images of: (a) a PS-*b*-PEO (42-11.5) self-assembled thin film formed on an n-doped Si substrate, (b) magnified image of the template, (c) array of PZT nanodots deposited using the PS-*b*-PEO thin film at 600 °C and (d) magnified image of PZT nanodots (inset shows cross-sectional TEM image of isolated nanodots).

The size, thickness, spacing and long-range ordering of the nanodots can be controlled by adjusting the molecular weight of any of the components in a BCP.[24] The size of an individual polymer block usually scales with molecular weight, i.e. a decrease in molecular weight reduces the size and/or spacing of polymer domains.[24] This hypothesis was utilized to reduce the size and thickness of the PZT nanodots generated on the Si substrates, by using the BCP PS-*b*-PEO (32-11), where the number-average molecular weight, (Mn) of PS was reduced to 32 kg mol^{-1}. The atomic force microscope (AFM) image of a self-assembled PS-*b*-PEO (32-11) thin film formed on an n-doped Si substrate (Figure 2(a)) shows that the ordering of the PS-*b*-PEO is significantly improved, while the size of the PEO domains (dark contrast) decreases to 17 nm. The thickness of the film is 25 nm as measured by optical ellipsometer. The ordering of block copolymers is driven by total free energy minimization, with enthalpic and entropic contributions. After spin coating, polar PEO layer preferentially wet the substrate surface (favourable PEO-substrate interactions) whilst PS will segregate to the air interface to form a PS-rich layer (PS has a lower surface energy, γPS = 33 mNm-1; γPEO = 43 mNm-1). Solvent annealing in toluene and toluene/water was used to induce long range-ordering and favor vertical cylinder orientation for (32-11) and (42-11.5) respectively. The value of χN (where, χ is the Flory-Huggins interaction parameter and N is the degree of polymerization) is 41.5 for (42-11.5) which is higher than that of (32-11) (33.3) implying higher thermodynamic driving force for micro phase separation, orientation and better degree of ordering. But solvent annealing in toluene for (42-11.5) causes cyclical structural transition between vertical and parallel orientation of PEO domains with annealing time.[32] Toluene imparts mobility and higher degree of swelling only in the PS component because of higher volume fraction of PS causes instability in the orientation. Thus toluene and water was used to impart mobility to both the blocks to stabilize the PEO cylinder orientation. Though both the systems has almost same molecular weight for PEO, the cylinder diameter becomes larger for (42-11.5) than (32-11) because of swelling of PEO domains in water environment. The swelling of the PEO domains also causes defects such as thickness undulation and interconnection between two domains which hamper the long range ordering of the film. As seen in Figure 2(a), the PS-*b*-PEO (32-11) thin film solvent annealed in toluene possesses high long-range ordering, as evident from the hexagonal arrangement of PEO block domains. A decrease in the diameter as well as depth of the PEO domains lead to a decrease in the size of the PZT nanodots formed, as the metals have a preferential affinity towards the hydrophilic PEO block. As shown in Figures 2(b) and (c), the PZT nanodots fabricated using the PS-*b*-PEO (32-11) thin film had smaller dimensions (~ 20 ± 5 nm in diameter, and ~ 10 nm in thickness) and a smaller mean center-to-center cylinder spacing (~ 32 nm) compared to the nanodots generated from the PS-*b*-PEO (42-11) template. The morphology of the nanodots formed using the PS-b-PEO (32-11) template was pyramidal compared to semi-spherical with the PS-*b*-PEO (42-11) template. The inset in Figure 2(c) shows the FFT pattern obtained for the arrays of PZT nanodots, which confirmed the hexagonal long-range ordering of the arrays. The coverage density of the PZT nanodots was ~ 68 × 10^9 nanodots per cm^{-2}, for the PS-*b*-PEO (32-11) template, which was greater than with the PS-*b*-PEO (42-11.5). This can be explained by the decrease in center-to-center cylinder spacing between the polymer blocks in (32-11) template.

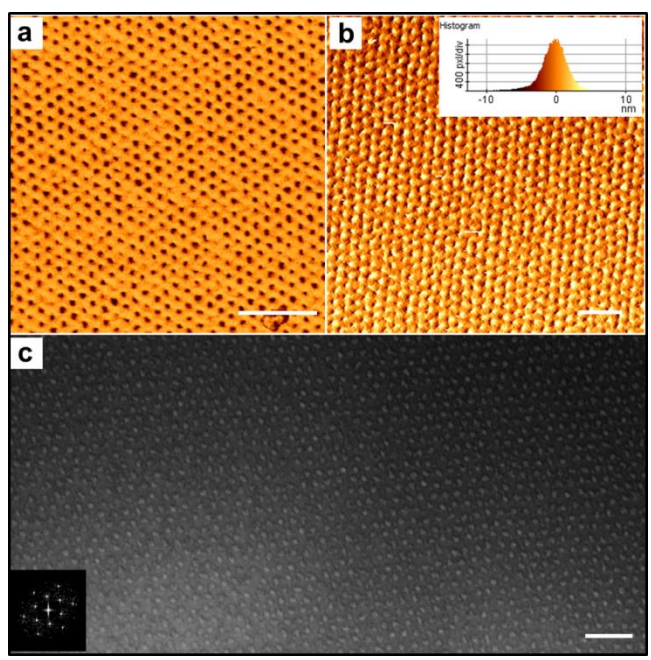

Figure 2. AFM topography image of: (a) a PS-*b*-PEO (32-11) self-assembled thin film formed on a n-doped Si substrate and (b) arrays of PZT nanodots formed using a PS-*b*-PEO (32-11) thin film (inset shows the histogram of the nanodot size). (c) Plan-

view SEM image of an array of PZT nanodots formed from a PS-*b*-PEO (32-11) template, the FFT pattern in the inset shows the hexagonal ordering of the nanodots. (Scale bars, 200 nm).

The formation of PZT nanodots using PS-*b*-PEO can be explained by the selective intra-molecular or intermolecular co-ordination between the metal ions (Pb^{2+}, Zr^{4+}, and Ti^{4+}) present in the precursor solution and the hydrophilic PEO chains present in the PS-*b*-PEO template. PEO is known to have a good affinity with the cationic species,[27,33] and the tendency towards multiple co-ordination is favored by its all-trans zigzag, or cis-helical, configuration (Figure 3).[33] It has previously been shown that hydrogen bonding between the additives and PEO chains in a BCP can enhance the selective dispersion and interaction of the additives in the PEO matrix.[34-37] Thus the Pb^{2+}, Zr^{4+}, and Ti^{4+} ions present in the precursor solution form dative bonds with the ether functional moieties (-O-) present in the PEO block, whilst being excluded from the hydrophobic PS block, eventually resulting in the nanodot formation.[27]

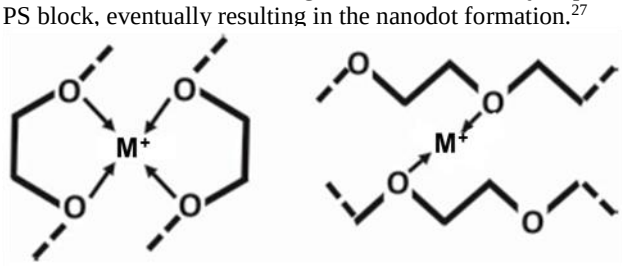

Figure 3. Schematic illustration of the possible metal cation (M^+)-PEO block co-ordination by means of the *cis*-helical and all-*trans* zig-zag geometry of the PS-b-PEO chains.[27]

Figure 4 shows an XRD pattern obtained for an array of PZT nanodots templated from a PS-*b*-PEO (42-11.5) polymer on an n-doped Si substrate. Diffraction peaks observed at $2\theta = 22$, 32.1, 38.2 were indexed to (001)/ (100), (110)/ (101) and (111) reflection planes of tetragonal pervoskite PZT, (PDF no. 33-0784). Similar XRD patterns were obtained for arrays of PZT nanodots template from a PS-*b*-PEO (32-11) polymer.

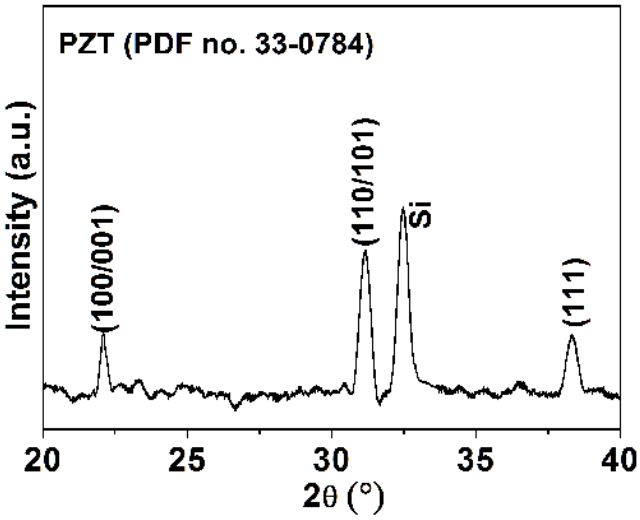

Figure 4. XRD pattern of arrays of PZT nanodots fabricated using a PS-*b*-PEO (42-11.5) template on an n-doped Si substrate; indexed to pervoskite PZT (PDF no. 33-0784).

In order to confirm the presence of a pervoskite phase, X-ray photoelectron spectroscopy (XPS) analysis was carried out on PZT nanodot samples. Figure 5 shows the XPS survey spectrum and the high resolution core-level spectra of individual metal ions from arrays of PZT nanodots produced using the PS-*b*-PEO (42-11.5) template. The XPS survey spectrum (Figure 5(a)) shows dominant peaks of Pb, Zr, Ti, O along with the Si peaks from the substrate, confirming that no contamination occurred during the PZT deposition process. Figures 5(b) to (e) shows the high resolution core-level XPS spectra with deconvoluted fits of Pb (4f), Zr (3d), Ti (2p), and O (1s) respectively. As observed in Figures 5(b) to (d), Pb, Zr, and Ti show only one spin-orbit doublet, indicating the presence of a single chemical environment in the PZT nanodots synthesized. The values of core-level binding energies obtained for each metal present in PZT nanodots were, Pb ($4f_{7/2}$) = 138.25 eV, and Pb ($4f_{5/2}$) = 143.11 eV, with a peak separation of 4.86 eV; Zr ($3d_{5/2}$) = 182.20 eV and Zr ($3d_{3/2}$) = 184.55 eV, with a peak separation of 2.35 eV; Ti ($3p_{3/2}$) = 458.81 eV and Ti ($3p_{1/2}$) = 464.25 eV, with a peak separation 5.44 eV. The O (1s) core-level spectrum was deconvoluted into two peaks, at 529.58 eV and 531.33 eV and were assigned to lattice oxygen and surface oxygen on the PZT nanodots respectively.[38] The observed binding energies were in good agreement with those previously reported for a pervoskite PZT chemical environment.[38]

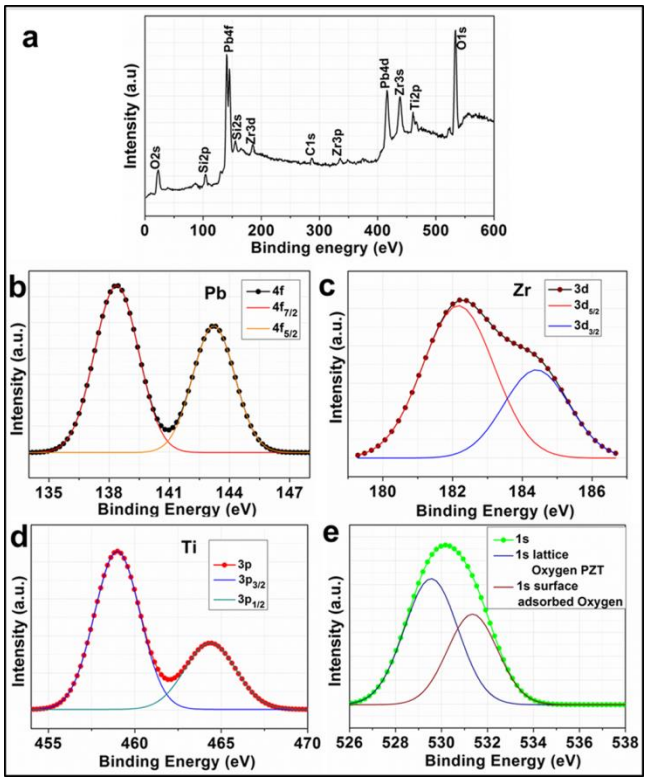

Figure 5. (a) XPS survey spectra of PZT nanodots fabricated using a PS-*b*-PEO (42-11) template on an n-doped Si substrate. Deconvoluted high resolution XPS spectra of: (b) Pb (4*f*), (c) Zr (3*d*), (d) Ti (3*p*) and (e) O (1*s*) from the PZT nanodots.

Piezoresponse force microscopy (PFM) was used to investigate the ferroelectric functionality of the arrays of PZT nanodots. Figure 6 shows (a) the piezoresponse topography, (b) and (d) the amplitude and (c) and (e) phase images of PZT nanodots formed from a PS-*b*-PEO (42-11.5) template, as measured by vertical PFM; the piezoresponse amplitude and phase provide information on the local electromechanical activity and the direction of local polarization, respectively.[39] The distinct bright and dark contrast in the piezoresponse amplitude images, shown in Figures 6(b) and (d), clearly highlight the presence of piezoelectric behavior in the individual PZT nanodots. The bright contrast is an indication of a large out-of-plane polarization response present in the nanodots, while the relatively dark contrast indicates less polarized regions.[39] PZT nanodots exhibited good piezoresponse over a large area (Figure 6(b)), with the majority of the dots showing a large out-of-plane piezoresponse. Previous articles have reported that tetragonal PZT films show a very high out of-plane response.[40]

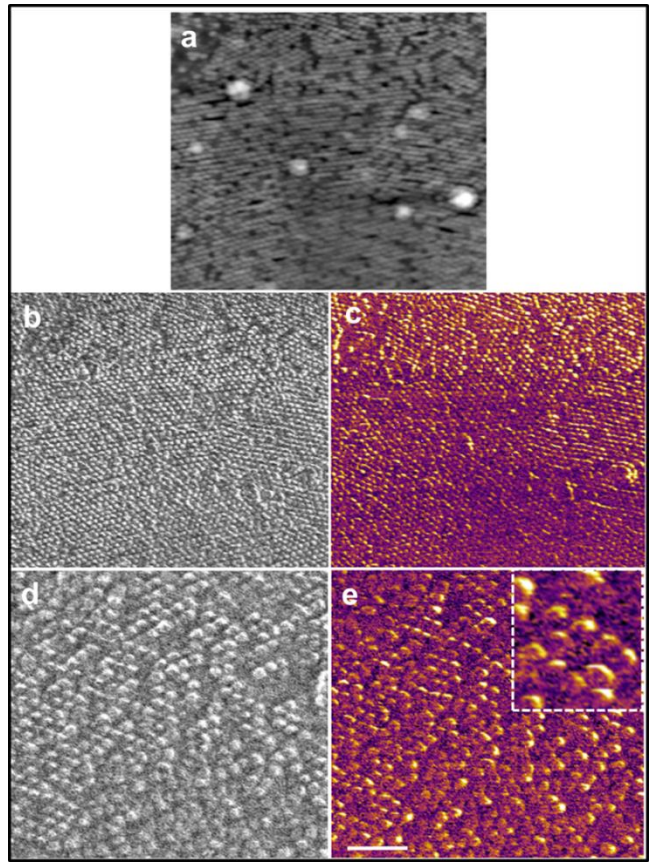

Figure 6. PFM images showing (a) topography, (b) amplitude and (c) phase profiles of PZT nanodot arrays fabricated using a PS-*b*-PEO (42-11) template on an n-doped Si substrate. (d, e) high resolution PFM amplitude and phase images of arrays of PZT nanodots (inset shows multi-domain structure). Scale bar, 200 nm.

The phase images in Figures 6(c) and (e) show that the ferroelectric domains present in PZT nanodots have a multi-domain structure as evident from the bright/dark color contrast. The orientation of the bright and dark contrast on the nanodots may also be indicative of a relationship between the PFM scan direction and piezoresponse in the nanodots. As the tip rises up over a nanodot, it gets a different piezoelectric "push" from when it runs down on the other side. The random orientation of ferroelectric domains can be explained by the pseudo-epitaxial polycrystalline nature of PZT nanodots and is common in polycrystalline PZT films.[41] This observation is supported by the TEM image (Figure 1(d)) and XRD pattern (Figure 4) obtained for PZT nanodot samples, where the dots show reflections from (110) and (111) directions, indicating that the crystallographic orientation in the sample is not constrained to one orientation and thus the formation of a multi-*a*/*c* domain (*a*-domain, parallel to the substrate plane; and *c*-domain, perpendicular to the plane) structure is expected. In Figure 6(c), some of the dots are composed of a single *c*-domain (orange contrast in top part), whilst dots at the bottom display multi-domains, with evidence of coupled phase contrasts in one dot. These phase contrast can be clearly seen in Figure 6(e) and in the magnified inset image.

Arrays of PZT nanodots fabricated using a PS-*b*-PEO (32-11) template also showed piezoelectric and ferroelectric responses.

Figures 7(a) and (b) show the PFM amplitude and phase images obtained for these arrays respectively. As seen in the PFM amplitude image (Figure 7(a)), most of the nanodots displayed a strong out-of-plane piezoresponse (bright contrast), while a few of them appeared dark. Close observation of the phase image (Figure 7(a)) shows the presence of multi-*a*/*c* domain structure with a high *c*-domain ratio. This observation is consistent with the PFM result obtained for PZT nanodots template from the PS-*b*-PEO (42-11.5) polymer. Significantly, these nanodots have a thickness ~10 nm and they still show ferroelectric behavior, which agrees with the previous reports.[42]

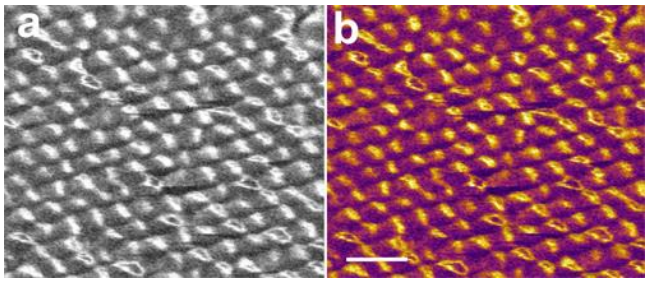

Figure 7. High resolution PFM (a) amplitude and (b) phase images of arrays of PZT nanodots fabricated using a PS-*b*-PEO (32-11) template on an n-doped Si substrate. Scale bar, 100 nm.

The polycrystalline and poly-domain character observed in the PZT nanodots (TEM image, Figure 1(d) insert) makes these arrays less ideal for ferroelectric memory cell applications, since currently the magnitude of switching cannot be well controlled.[43] Mono-domain structures could possibly be achieved by epitaxial growth of the nanodots on suitable substrates. Nevertheless, the BCP template-assisted approach described in this paper has great potential for producing highly ordered 2D arrays of ferroelectric nanodots. The same methodology can also be extended to fabricate laterally ordered ferroelectric and piezoelectric nanowire patterns.

CONCLUSION

In summary, a simple method for the fabrication of highly ordered arrays of PZT nanodots using self-assembled block copolymer templates was demonstrated. PZT nanodots with lateral widths and thicknesses as small as 20 nm and 10 nm respectively were prepared by PS-*b*-PEO polymer templates. The hexagonal long-range ordering of these nanodots was improved by decreasing the molecular weight of the polystyrene (PS) block used in the PS-*b*-PEO template. XRD and XPS analysis confirmed the pervoskite structure of PZT nanodots synthesized. PFM studies on individual PZT nanodots confirmed the presence of piezoelectric and ferroelectric behavior.

AUTHOR INFORMATION

Corresponding Author

* Justin D. Holmes, E-mail: j.holmes@ucc.ie, Tel: +353 (0)21 4903608; Fax: +353 (0)21 4274097.

ACKNOWLEDGMENT

This work was supported by Science Foundation Ireland (SFI) (Grants: 07/SRC/I1172 and 08/CE/I1432). This research was also enabled by the Higher Education Authority Program for Research in Third Level Institutions (2007-2011) via the INSPIRE program. The authors acknowledge the facilities of, and technical assistance from the staff at, Electron Microscopy and Analysis Facility (EMAF) at Tyndall National Institute. Also, thanks to Pete Fleming for his assistance with XPS analysis.

REFERENCES

(1) Ionescu, A. M. *Nat Nano* **2012**, *7*, 83.
(2) Bibes, M. *Nat Mater* **2012**, *11*, 354.
(3) Lee, W.; Han, H.; Lotnyk, A.; Schubert, M. A.; Senz, S.; Alexe, M.; Hesse, D.; Baik, S.; Gosele, U. *Nat Nano* **2008**, *3*, 402.
(4) *The International Technology Roadmap for Semiconductors: 2011 Edition, Emerging research materials and Emerging research devices; http://www.itrs.net/Links/2011ITRS/2011Chapters/2011ERM.pdf, http://www.itrs.net/Links/2011ITRS/2011Chapters/2011ERD.pdf*.
(5) Alexe, M.; Harnagea, C.; Hesse, D.; Gosele, U. *Appl. Phys. Lett.* **1999**, *75*, 1793.
(6) Alexe, M.; Harnagea, C.; Visinoiu, A.; Pignolet, A.; Hesse, D.; Gosele, U. *Scripta Mater.* **2001**, *44*, 1175.
(7) Shin, H.-J.; Choi, J. H.; Yang, H. J.; Park, Y. D.; Kuk, Y.; Kang, C.-J. *Appl. Phys. Lett.* **2005**, *87*, 113114.
(8) Kang, S. J.; Bae, I.; Shin, Y. J.; Park, Y. J.; Huh, J.; Park, S.-M.; Kim, H.-C.; Park, C. *Nano Lett.* **2010**, *11*, 138.
(9) Kusuma, D. Y.; Nguyen, C. A.; Lee, P. S. *The Journal of Physical Chemistry B* **2010**, *114*, 13289.
(10) Scott, J. F. *Integrated Ferroelectrics* **2000**, *31*, 139.
(11) Lee, J.-S.; Lee, B.-I.; Joo, S.-K. *Integrated Ferroelectrics* **2000**, *31*, 149.
(12) Marshall, J. M.; Dunn, S.; Whatmore, R. W. *Integrated Ferroelectrics* **2004**, *61*, 223.
(13) Shen, Z.; Chen, Z.; Lu, Q.; Qiu, Z.; Jiang, A.; Qu, X.; Chen, Y.; Liu, R. *Nanoscale Research Letters* **2011**, *6*, 474.
(14) Hu, Z.; Tian, M.; Nysten, B.; Jonas, A. M. *Nat Mater* **2009**, *8*, 62.
(15) Son, J. Y.; Shin, Y.-H.; Ryu, S.; Kim, H.; Jang, H. M. *J. Am. Chem. Soc.* **2009**, *131*, 14676.
(16) Szafraniak, I.; Harnagea, C.; Scholz, R.; Bhattacharyya, S.; Hesse, D.; Alexe, M. *Appl. Phys. Lett.* **2003**, *83*, 2211.
(17) Szafraniak, I.; Chu, M. W.; Harnagea, C.; Scholz, R.; Hesse, D.; Alexe, M. *Integrated Ferroelectrics* **2004**, *61*, 231.
(18) Kim, J.; Hong, J.; Park, M.; Zhe, W.; Kim, D.; Jang, Y. J.; Kim, D. H.; No, K. *Adv. Funct. Mater.* **2011**, *21*, 4277.
(19) Ma, W.; Harnagea, C.; Hesse, D.; Gosele, U. *Appl. Phys. Lett.* **2003**, *83*, 3770.
(20) Ma, W.; Hesse, D.; Gösele, U. *Small* **2005**, *1*, 837.
(21) Wenhui, M.; Dietrich, H.; Ulrich, G. *Nanotechnology* **2006**, *17*, 2536.
(22) Vrejoiu, I.; Alexe, M.; Hesse, D.; Gösele, U. *Adv. Funct. Mater.* **2008**, *18*, 3892.
(23) Kim, J. K.; Yang, S. Y.; Lee, Y.; Kim, Y. *Prog. Polym. Sci.* **2010**, *35*, 1325.
(24) Kim, H.-C.; Park, S.-M.; Hinsberg, W. D. *Chem. Rev.* **2009**, *110*, 146.
(25) van Zoelen, W.; Vlooswijk, A. H. G.; Ferri, A.; Andringa, A.-M.; Noheda, B.; ten Brinke, G. *Chem. Mater.* **2009**, *21*, 4719.
(26) Kim, Y.; Han, H.; Kim, Y.; Lee, W.; Alexe, M.; Baik, S.; Kim, J. K. *Nano Lett.* **2010**, *10*, 2141.
(27) Ghoshal, T.; Maity, T.; Godsell, J. F.; Roy, S.; Morris, M. A. *Adv. Mater.* **2012**, *24*, 2390.
(28) Izyumskaya, N.; Alivov, Y. I.; Cho, S. J.; Morkoç, H.; Lee, H.; Kang, Y. S. *Crit. Rev. Solid State Mater. Sci.* **2007**, *32*, 111.
(29) Zhang, Q.; Whatmore, R. W. *J. Appl. Phys.* **2003**, *94*, 5228.
(30) Whatmore, R. W.; Zhang, Q.; Huang, Z.; Dorey, R. A. *Mater. Sci. Semicond. Process.* **2002**, *5*, 65.
(31) Muralt, P.; Maeder, T.; Sagalowicz, L.; Hiboux, S.; Scalese, S.; Naumovic, D.; Agostino, R. G.; Xanthopoulos, N.;

Mathieu, H. J.; Patthey, L.; Bullock, E. L. *J. Appl. Phys.* **1998**, *83*, 3835.
(32) Mokarian-Tabari, P.; Collins, T. W.; Holmes, J. D.; Morris, M. A. *ACS Nano* **2011**, *5*, 4617.
(33) Evans, C. C.; Bates, F. S.; Ward, M. D. *Chem. Mater.* **1999**, *12*, 236.
(34) Park, S.; Lee, D. H.; Xu, J.; Kim, B.; Hong, S. W.; Jeong, U.; Xu, T.; Russell, T. P. *Science* **2009**, *323*, 1030.
(35) Lin, Y.; Daga, V. K.; Anderson, E. R.; Gido, S. P.; Watkins, J. J. *J. Am. Chem. Soc.* **2011**, *133*, 6513.
(36) Epps, T. H.; Bailey, T. S.; Waletzko, R.; Bates, F. S. *Macromolecules* **2003**, *36*, 2873.
(37) Daga, V. K.; Watkins, J. J. *Macromolecules* **2010**, *43*, 9990.
(38) Wakiya, N.; Kuroyanagi, K.; Xuan, Y.; Shinozaki, K.; Mizutani, N. *Thin Solid Films* **2000**, *372*, 156.
(39) Kholkin, A.; Kalinin, S.; Roelofs, A.; Gruverman, A. Review of Ferroelectric Domain Imaging by Piezoresponse Force Microscopy. In *Scanning Probe Microscopy: Electrical and Electromechanical Phenomena at the Nanoscale*; Kalinin, S., Gruverman, A., Eds.; Springer New York, 2007; pp 173.
(40) Harnagea, C.; Pignolet, A.; Alexe, M.; Hesse, D. *Integrated Ferroelectrics* **2002**, *44*, 113.
(41) Wu, A.; Vilarinho, P. M.; Shvartsman, V. V.; Suchaneck, G.; Kholkin, A. L. *Nanotechnology* **2005**, *16*, 2587.
(42) Chu, M.-W.; Szafraniak, I.; Scholz, R.; Harnagea, C.; Hesse, D.; Alexe, M.; Gosele, U. *Nat Mater* **2004**, *3*, 87.
(43) Rodriguez, B. J.; Gao, X. S.; Liu, L. F.; Lee, W.; Naumov, II; Bratkovsky, A. M.; Hesse, D.; Alexe, M. *Nano Lett.* **2009**, *9*, 1127.
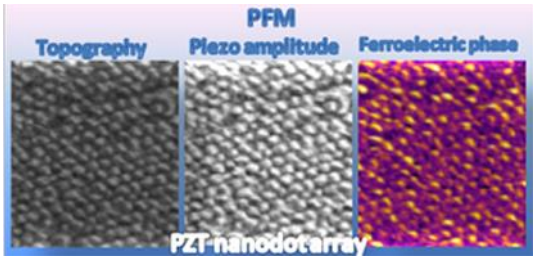
Insert Table of Contents artwork here